Ashish Yadav

Journal of Physics: Condensed Matter

PAPER

Overlapping large polaron tunnelling in lanthanum silicate oxyapatite

To cite this article: Ashishkumar Yadav *et al* 2023 *J. Phys.: Condens. Matter* **35** 095702

J. Phys.: Condens. Matter **35** (2023) 095702 (8pp) https://doi.org/10.1088/1361-648X/acad53

Overlapping large polaron tunnelling in lanthanum silicate oxyapatite

Ashishkumar Yadav[1], Priyanka A Jha[1,*], Pardeep K Jha[1], Neetu Jha[2] and Prabhakar Singh[1,*]

[1] Department of Physics, Indian Institute of Technology (Banaras Hindu University) Varanasi, Varanasi 221005, India
[2] Department of Physics, Institute of Chemical Technology Mumbai 400019, India

E-mail: priyankajha.dce@gmail.com and psingh.app@iitbhu.ac.in

Received 2 August 2022, revised 17 November 2022
Accepted for publication 20 December 2022
Published 28 December 2022

Abstract

Amongst the various fast ion conductors, lanthanum excess lanthanum silicate oxyapatite ($La_{10-\alpha}(SiO_4)_6O_{2+\delta}$) has shown higher oxide ion conductivity with lower activation energy. On the other hand, the activation energy increases with La vacancies (La at 4f site). In the present work, La site is altered with Ca to form $(La_{1-x}Ca_x)_{9.67}(SiO_4)_6O_{2+\delta}$ ($x = 0.0, 0.05, 0.10$ and 0.15) with minimum oxygen non-stoichiometry and studied the hopping/tunnelling mechanism with the Ca substitution. The elemental content obtained from Rietveld refinement of the x-ray diffractograms suggests La deficiency with minimum oxygen deficiency. Further, XPS and TGA studies confirm the formation of La deficient samples. Temperature and frequency dependent ac conductivity in the temperature range (548–973 K) suggests that the conduction takes place via overlapping large polaron tunnelling. Further, the tunnelling distance and polaron radii as a function of temperature and frequency are observed to be altered with Ca and affecting the ion conducting channel through the elongation of La(6 h) triangles. Our study suggests the phononic contribution play a pivotal role in ionic transport.

Supplementary material for this article is available online

Keywords: polarons, ion conductors, silicates, apatite

(Some figures may appear in colour only in the online journal)

1. Introduction

Solid oxide ion conductors play a significant role in electricity conversion devices (solid oxide fuel cells (SOFCs)) as an alternative energy [1]. SOFC is an electrochemical device which requires high temperature (>1000 K) for its operation [1]. The recent surge in the energy demand comes from the domestic sector where high temperature devices are generally restricted, this makes SOFC out of contest as a popular choice of portable alternative energy sources. Low temperature (working between 500 and 800 K) fast oxide ion conductors (FOICs) can solve this problem [1, 2]. The ionic conductivity of the high temperature FOICs generally decreases sharply with decrease in the temperature [2] hence such FOICs cannot be used in low temperature SOFC (IT and LT-SOFC). Thus, there is quest for FOICs at low temperatures.

The apatite based FOICs (discovered by Nakayama in 1995) [3], like perovskite based FOICs [4–6] showed high ionic conductivity in low temperature regime [2, 7–14]. Among these FOICs, due to its anisotropic ion conduction ($\sigma_c^{||}/\sigma_c^{\perp} > 10$), lanthanum silicate oxyapatite, i.e. $La_{10-\alpha}^{3+}(SiO_4)_6^{4-}O_{2+\delta}^{2-}$ (LSO) is one of the most interesting materials [15, 16]. In polycrystalline samples, grain alignment

* Authors to whom any correspondence should be addressed.

and doping are the two common methods to get the desired properties in the sample, the same has been employed by various research groups in the last few years [2, 7, 8, 10–13, 16–21]. Various doping such as Al, Mg at B-site and alkaline earth and rare Earth substitutions at A-site have been done in order to get conductivities in the range of 1 S cm^{-1} but unfortunately, conductivity is achieved in the range of 10–50 mS cm^{-1} [7–11, 13, 14, 16, 19, 20, 22]. To explain this the two kind of conduction mechanism, namely, push–pull [17] and interstitial [9, 18] are well described for the oxyapatites. In the push–pull conduction mechanism, interstitial oxygen cooperatively migrates with O4 to the most stable interstitial O site with the lowest potential barrier of 0.01 eV with site energies in the range of 0–0.25 eV. Thus, it is supposed to occur in the ideal perfect crystal lattice with no defects and no La vacancies and migration is comparable to short range hopping in the stable zone. In the other mechanism where O_2 oxygen is involved, the potential barrier is 0.53 eV with the site energy 0.82 eV [23]. The long range conduction mechanism consists of long pathways in the O4 column with the cooperative interstitial mechanism. It leads to strong anisotropy in the oxygen ion conduction being reported by Nakayama in 2013 [24]. Various experiments [9] and theoretical studies [17] predict that O_{int} (interstitial oxygen) promotes cooperative movements between the O4 ion and excess oxygen is introduced as interstitial charge carriers to maintain electrical neutrality with La ions. There are four channels proposed for the conduction. Channels nos. 1 and 2 are formed by the oxygen vacancies in between La(4f)–O4, channel no. 3 is nearest to the Si vacancy site and channel no. 4 is linked to the formation of oxygen Frenkel defects [17, 18]. Despite of these studies, the dynamics which can explain the ion conduction alteration with structural disorder (polaronic hopping) is still scarce at large in spite of the fact that there is correlation between ion diffusion and polaron prevalence in ionic conductors [25–27].

In ionic conductors conduction is a prototype of polarons and the conduction is possible due to the jump of mobile ions with a large phonon amplitude. Further, the lowering of activation energy assists the enhanced phonon amplitudes which assist the jump of mobile ions and ion conduction [28]. Thus, there is scope of conductivity enhancement in polycrystalline LSO by understanding the role of phononic contributions. In order to check the correlation between polaron hopping and ion diffusion, we are here investigating the alteration in the structural disorder and dynamics with Ca-substitution in LSO. To investigate this correlation, we have analysed the structural, low frequency ($10\,s^{-1} < \omega \leqslant 10^6 s^{-1}$) conductivity, optical absorption, valence band edge through photoemission spectroscopy and field dependent conductivity.

2. Results and analysis

The structural and dynamic disorders are important feature for ion conduction. In order to understand the modification caused by Ca-substitution at La-site in $La^{3+}_{10-\alpha}(SiO_4)^{4-}_6 O^{2-}_{2+\delta}$; with $\alpha = 0.33$ system and its influence on the ion transport behaviour, we performed structural and electrical characterization in details (see supplementary). The Rietveld analysis suggest hexagonal P63/m symmetry for $x = 0, 0.05, 0.1$ and 0.15 in $(La^{3+}_{1-x}Ca^{2+}_x)_{9.67}(SiO_4)^{4-}_6 O^{2-}_{2+\delta}$. However, some low intensity reflection of SiO_x appears with substitution which is visible for $x = 0.15$. The elemental content obtained from Rietveld refinement of the XRD, XPS and TGA confirm the formation of La deficient samples (for further detail about structural parameters see supplementary). Here, the ratio of area of peaks corresponding to metal-O and metal-OH is observed to decrease with the increase in x and showing the decrease in oxygen vacancy concentration with x. Thus, oxygen content is observed to increase and vacancy is observed to decrease with the increase in x. Further, Na KLL Auger peak is observed in $x = 0.0$ and with the increase in x, Auger peak diminishes. Simultaneously, intensity of satellite peak in Ca 2p spectra is increasing with x due to metal ligand interaction, i.e. interaction of s-orbital of Ca and p-orbital of O (s–p interaction). In addition, the formation of $La(OH)_3$ suggests the formation of La vacancies and the samples are found to be La and Si deficient from the occupancies observed from the Rietveld refinement. Thus, the formation of oxygen/lanthanum and silicon vacancies has been analyzed through thermogravimetric analysis in N_2 atmosphere. A gradual mass loss with two kinks (at ~500 and 800 K) are observed in thermogravimetric curves and these kinks correspond to the weight loss due to La. The La deficiency observed is in accordance with the La content estimated from XPS and Rietveld refinement (details are in supplementary). From impedance spectroscopy, we observed diffusive spectra at low frequency in all samples while at high frequency end the behaviour almost resistive with very low impedance which is signature of ion-diffusion [29].

The apatite structure does not go under structural phase transition till high temperature as high as 1473 K, therefore electrical behaviour till 1000 K can be easily found in correlation with structure at room temperature. The conductivity–frequency–temperature ($\sigma - \omega - T$) plots are drawn for each sample. These frequency ($10\ s^{-1} < \omega \leqslant 10^6 s^{-1}$) dependent conductivity isotherms (548–973 K) (see supplementary) are fitted with Jonsher Power law(JPL) [30]:

$$\sigma = \sigma_{dc}(1 + (\omega/\omega_h)^p). \quad (1)$$

Through the fitting of conductivity isotherms with JPL, dc conductivity (σ_{dc}), hopping frequency (ω_h) and exponent (p) are extracted.

2.1. Temperature dependence conduction behaviour

2.1.1. dc Conductivity. Figure 1 σ_{dc}–T plot for all samples it is clearly visible that with x conductivity increase up to $x = 0.1$ there after it decreases for $x = 0.15$. The conductivity in these apatites strongly depends on the activation energy. Therefore, σ_{dc}–T curves are fitted with Arrhenius relation ($\sigma = \sigma_0 \exp(-E_a/k_B T)$; solid red line) and also with nearest

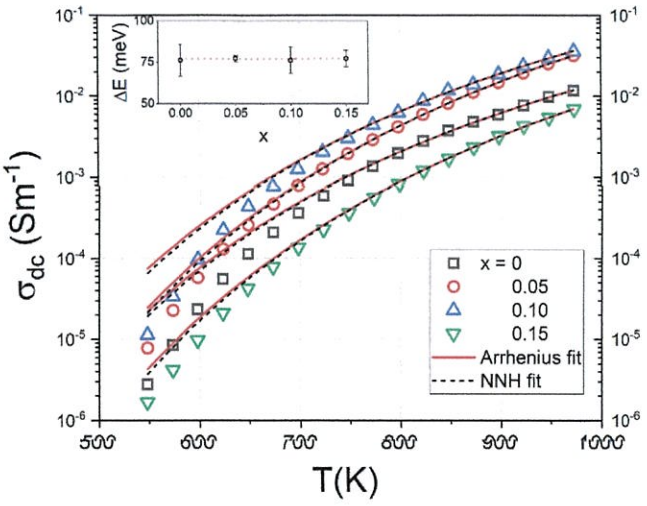

Figure 1. Arrhenius and NNH fitting of σ_{dc}–T curves for $x = 0, 0.05, 0.1$ and 0.15 in $(La^{3+}_{1-x}Ca^{2+}_{x})_{9.67}(SiO_4)^{4-}_{6}O^{2-}_{2+\delta}$ system. (Inset) shows the difference in the two activation energies is ΔE ~75 meV.

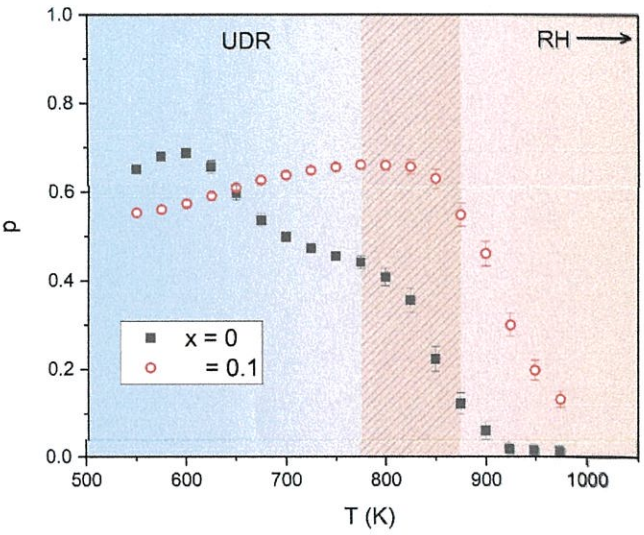

Figure 2. The universal exponent (p)–temperature (T) plot for $x = 0, x = 0.1$ in $(La^{3+}_{1-x}Ca^{2+}_{x})_{9.67}(SiO_4)^{4-}_{6}O^{2-}_{2+\delta}$ system.

neighbour hopping (NNH) model ($\sigma T = \sigma_0 \exp(-E_a/k_B T)$, dashed black line). For $T > 700$ K both fitting match well, however NNH fitting has better correlation ($R^2 > 0.999$) with experimental data which confirm nearest neighbour hopping in these samples. Here, with substitution of Ca, no particular trend could be observed for activation energy as observed in the structural and microstructural parameters. The activation energies (NNH) are $E_h \sim 0.76, 0.85, 0.74$ and 0.88 eV respectively. However the interesting feature is the difference in the two activation energies is ΔE ~75 meV (figure 1 (inset)). It is necessary to mention that 75 meV is a significant value which indicates oxygen vacancy assisted polaron conduction [31, 32]. However, in the present context, it is the difference which is 75 meV and beyond our present understanding. The high activation energy (0.85 eV) for $x = 0.05$ is due to porosity [33, 34] as observed in microstructures, while for $x = 0.15$, it is due to SiO_x phase, which provide more scattering thus more resistance is offered. Thus hereafter, we are comparing the hopping conduction mechanism in the samples with same activation energy, i.e. $x = 1.0$ ($E_h \sim 0.74$ eV) with undoped LSO, i.e. $x = 0$ ($E_h \sim 0.76$ eV).

2.1.2. The universal exponent 'p'. The universal exponent (p) behaviour can suggest how frequency dependence of conduction behaviour is altering with thermal activation. Therefore p–T curves are drawn for the two samples, i.e. $x = 0.0$ and $x = 0.1$ (figure 2). It is observed for both the samples that the exponent is continuously decreasing for temperature range (773–873 K). Beyond 873 K, $p \to 0$ suggesting diffusion and hence transport is almost frequency and temperature independent for $x = 0.0$. However, $p \to 0$ at a higher temperature >1000 K for $x = 0.1$. Consequently lead to ions hopping between two sites and does not have any information of the previous site, therefore random hopping is approached by both the samples once thermal energy exceeds ~75 meV. The major difference between two samples is appearing for temperature 548 K > T > 773 K. Here both the samples show the universal dielectric relaxation [30]. For $x = 0$, there is maxima at 598 K with $p \sim 0.7$ while for $x = 0.1$, there is maxima at 823 K with $p \sim 0.65$. Thus, the exponent behaviors for $x = 0$, suggests overlapping large polaron tunnelling (OLPT) while for $x = 0.1$ conduction is appearing due to correlated barrier hopping (CBH) and OLPT [35] which will be verified later. Nevertheless, $p < 1$ suggests the sublinear behaviour for both the samples.

2.2. Frequency dependent conductivity behaviour

2.2.1. The exponent parameter (s). The shape of σ_{dc}–T curves (figure 1) hints for quantum mechanical tunneling (QMT), CBH and OLPT [35]. The limitation with the universal exponent p is that it itself is not frequency dependent while the tunneling process is assisted by phonon interaction [35]. In the QMT and OLPT models, the exponent decreases with frequency while in the CBH phenomenon, the exponent increases with frequency. However QMT is a temperature independent process [35]. Thus we require other formalism for exponent which must be frequency and temperature dependent, for this we extracted the exponent parameter (s):

$$s = \frac{d \ln \sigma(\omega)}{d \ln \omega}. \quad (2)$$

The variation of s for the two samples are shown in the T–ω contour plot (figure 3). For both samples, the parameter 's' is frequency as well as temperature dependent. For $x = 0$, it is observed that with temperature s-value increases from ~0.86 to ~0.95, while for $x = 0.1$ s-value increases from ~0.92 to ~0.97. Here it is important to mention that the temperature dependence of 's' is not similar to the behaviour of universal

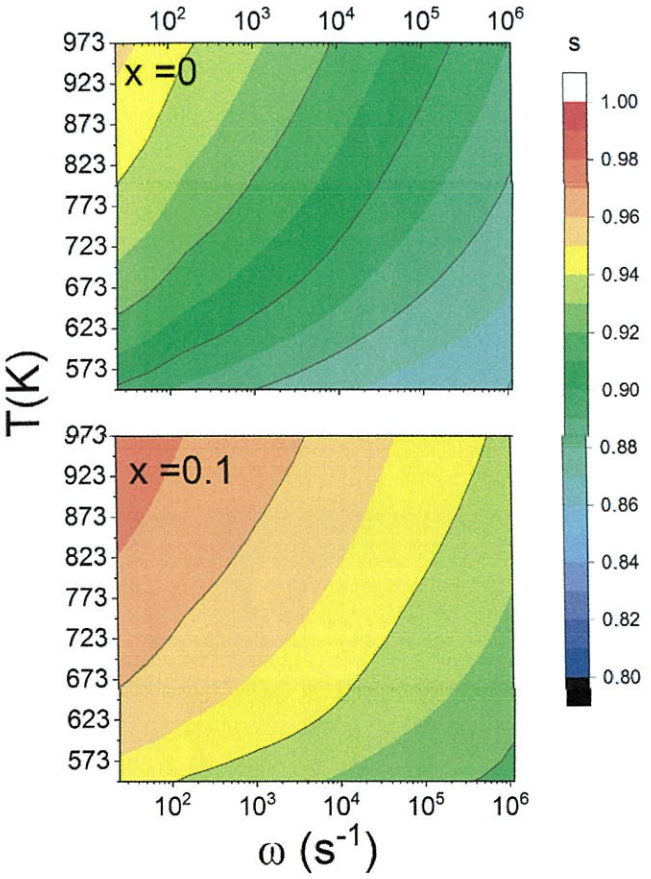

Figure 3. Two dimensional contour plot of s versus T and ω for $x = 0, x = 0.1$ in $(La^{3+}_{1-x}Ca^{2+}_{x})_{9.67}(SiO_4)^{4-}_{6}O^{2-}_{2+\delta}$ system.

exponent 'p'. As far as frequency dependence is concerned, the s-value decreases with frequency for both the samples. This suggests thermal activation favours some trapped charge carriers to hop between sites with unequal barrier height, therefore possibility of CBH and QMT is ruled out. However, we fitted the s–T curve (at $\omega(s^{-1}) \simeq 10^2$, 10^3, 10^4, 10^6) with CBH, QMT and OLPT and found that curves are well fitted with OLPT [36] (equation (3)) (figure 4):

$$s = 1 - (1/R')\frac{4 + 6/R_E}{(1 + 1/R_E)^2}, \tag{3}$$

here r_0', R' and R_E are reduced quantities which are defined as per equation (4):

$$\text{here } 1/R_E \equiv \beta E_{h0} r_0'/R'^2, r_0' = 2\alpha r_0 R' = 2\alpha R. \tag{4}$$

Further, $\beta \equiv 1/k_B T$, $E_{h0} = E_h/(1 - r_0/R)$, here r_0 is polaron radius, R is tunneling distance and E_h is hopping energy.

Here a function $\mathscr{F}(\omega, T)$ is defined as per equation (6) for tunnelling distance (R) expressed by equation (6):

$$\mathscr{F}(\omega, T) \equiv ln(\omega_h/\omega) - \beta E_{h0}, \text{where} \beta \equiv 1/k_B T, \tag{5}$$

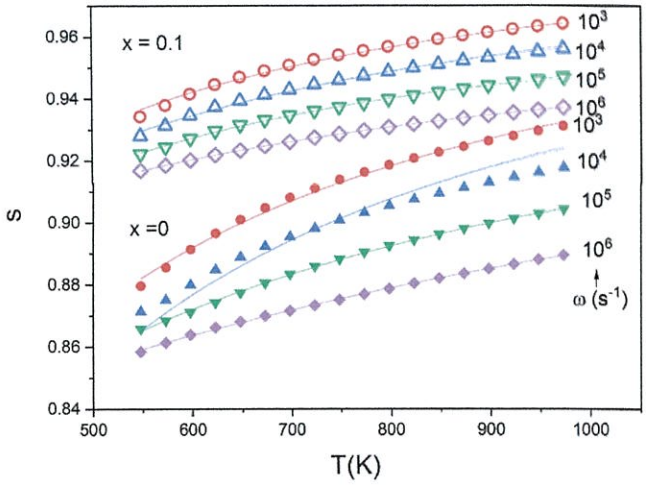

Figure 4. Overlapping large polaron tunnelling (OLPT) fitting of parameter s–T curves at $\omega = 10^3$, 10^4, 10^5 and $10^6(s^{-1})$ for $x = 0$ (filled), $x = 0.1$ (open) in $(La^{3+}_{1-x}Ca^{2+}_{x})_{9.67}(SiO_4)^{4-}_{6}O^{2-}_{2+\delta}$ system.

$$R(\omega) \equiv R = \frac{1}{4\alpha}\mathscr{F}(\omega, T) + \left\{\mathscr{F}^2(\omega, T) + 8\alpha r_0 \beta E_{h0}\right\}^{1/2}. \tag{6}$$

We observed that after fitting the exponent 's' with the OLPT model and using equations (4)–(6), the tunnelling distance (R), polaron radius (r_0) are extracted. Figure 5(a) shows the variation of R with frequency and (b) shows the variation of E_{h0} with R for $x = 0.0$ and 0.1. It is observed that the tunnelling distance reduces with the increase in frequency. The smallest tunnelling distance is observed at $\omega = 10^6$ s^{-1}(3.70 Å for $x = 0$. and 2.39 Å for $x = 0.1$), which is greater than La1-O3 bond lengths 'a' ($\lesssim$2.3 Å). Further, the polaron radii at frequency $\omega = 10^6$ s^{-1} for $x = 0$ sample is 19.28 Å and for the $x = 0.1$ sample, it is 4.31 Å, i.e. $r_0 > a$. Moreover, it can also be seen (figure 5(b)) that at lowest frequency, R is maximum and E_{h0} is minimum. Further, with the increase in frequency, E_{h0} is increasing. It is evident that hopping energy decreases with the tunnelling distance but the spatial extension of polarons is much larger for $x = 0.1$. It indicates the overlap of potential wells of the neighbouring sites because of long range Coulomb interaction [35] Further, extracted value of Frohlich coupling constant α is very high >3 and nearly similar for both samples, indicating strong electron–phonon coupling. This correlation between hopping energy and polaron radius with massive polaron formation suggests the ionic nature of the compounds [37].

2.3. Optical absorption

To get energetics of large polaron formation in these two samples, we have performed the optical absorption study. The threshold for the photo dissociation of large polarons is estimated at $3E_P$, where at E_P is (electronic portion of) large polaron binding energy [38, 39]. The estimated value of $E_P \sim 1.13$ eV for both the samples. The normalised optical (large polarons) absorption spectrum for $x = 0$ and 0.1 is plotted (figure 6(a))

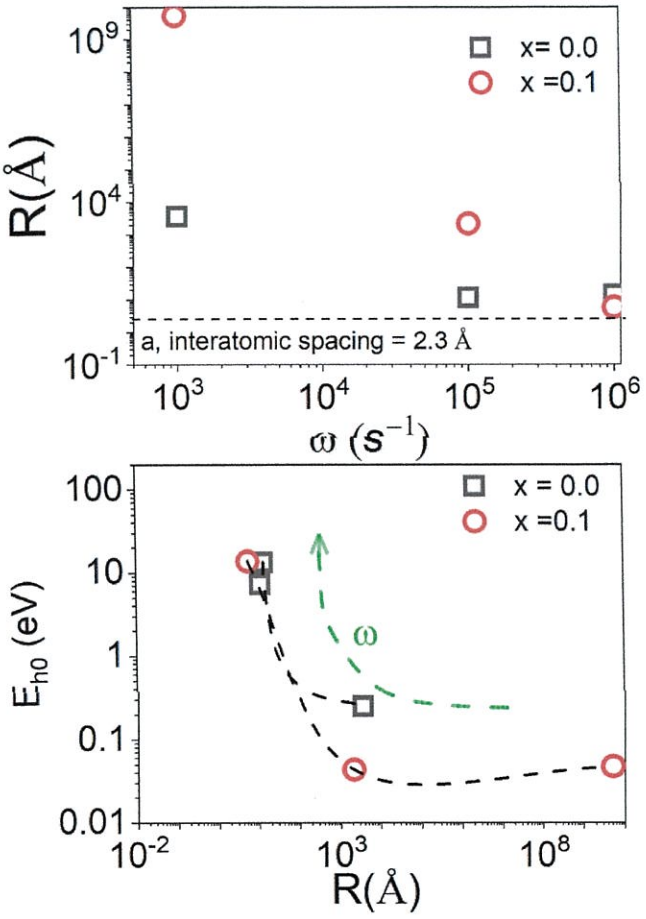

Figure 5. (a) Tunneling distance with frequency and (b) hopping energy with tunnelling distance at $\omega = 10^3$, 10^5 and $10^6(s^{-1})$ for $x = 0$ (square), $x = 0.1$ (circle) in $(La^{3+}_{1-x}Ca^{2+}_{x})_{9.67}(SiO_4)^{4-}_{6}O^{2-}_{2+\delta}$ system (lines are a glide to eye).

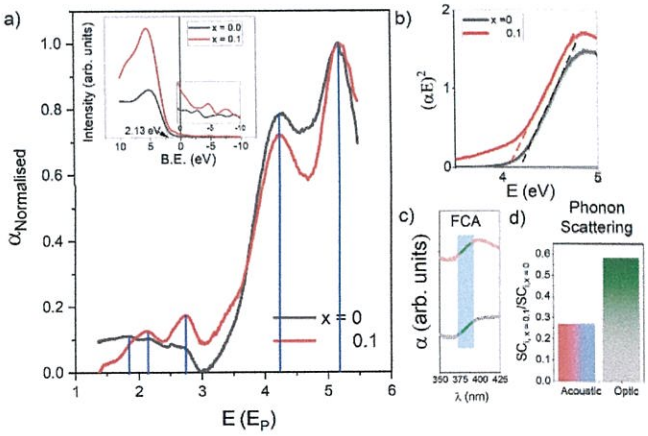

Figure 6. (a) Variation of normalised optical (large polaron's) absorption for $x = 0$ and 0.1 in $(La^{3+}_{1-x}Ca^{2+}_{x})_{9.67}(SiO_4)^{4-}_{6}O^{2-}_{2+\delta}$ system. (Inset) Valence band spectra using XPS study for both the samples along with zoomed valence band spectra in the negative binding energy region and (b) Tauc plots for direct band gap is estimated ~4.2 and 4.05 eV respectively suggested wider exciton energy for $x = 0.1$. (c) Free carrier absorption (FCA) fitting of the absorption obtained from UV-visible measurement for acoustic and optical phonon contributions. (d) Ratio of phononic scattering coefficient (i = acoustic and optical phonon contributions) for $x = 0.1$ and $x = 0.0$.

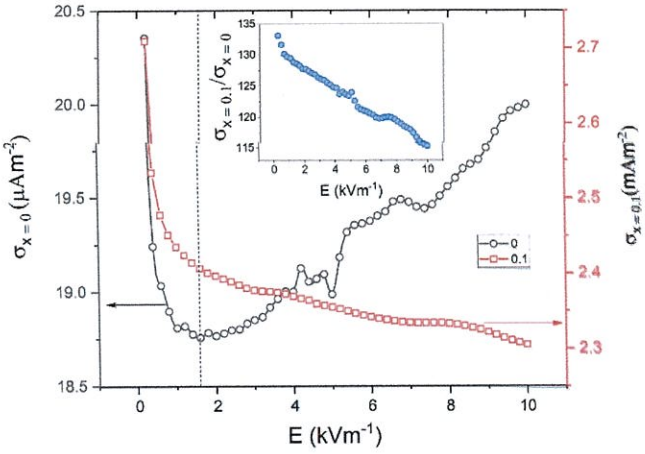

Figure 7. Field dependent conductivity for $x = 0$ and 0.1 in $(La^{3+}_{1-x}Ca^{2+}_{x})_{9.67}(SiO_4)^{4-}_{6}O^{2-}_{2+\delta}$ system, inset shows the ratio of conductivity for $x = 0.1$ and $x = 0.0$.

in terms of E_P. We can see some small absorption peaks for photon energy $E < 3E_P$, while strong absorption for $E > 3E_P$. For $E < 3E_P$, carrier absorption indicates phonon–electron interaction and therefore absorption is due to photoexcitation of polarons to bound states in the deformabale ion continuum. Before going into further details, it would be helpful to get some idea of electronic band structure. For this we have inspected valence band (VB) spectra using XPS study (figure 6(a) (inset)) and observed VB edge at ~2.13 eV from fermi level (E_f). We can see some photoemission at fermi level which is due to mobility transfer attributing to polarons [40]. Interestingly, photoemission is higher for $x = 0.1$ like optical absorption indicates higher mobility. Also, the direct band gap is estimated (from Tauc plots; figure 6(b)) ~4.2 and 4.05 eV, respectively, suggesting the lowering of conduction band edge for $x = 0.1$. This is due to the interaction of (Ca)s and O(p) electrons (s–p interaction, see supplementary figure S4 and its description). Further, to get the relative phonon contribution in these two samples, the data is fitted with free carrier absorption (FCA) equation $\alpha = \alpha_{AP}\lambda^{1.5} + \alpha_{OP}\lambda^{2.5} + \alpha_{IS}\lambda^{3.5} \approx \alpha_{AP}\lambda^{1.5} + \alpha_{OP}\lambda^{2.5}$ (if $\alpha_{IS} \to 0$) (figure 6(c)) [41] and found that scattering coefficient (SC) due to optical phonon scattering is reduced to ~1/2 while acoustic phonon scattering is reduced to nearly ~1/4 for $x = 0.1$. This explains the larger tunneling distance for $x = 0.1$ in acoustic frequency excitation (figure 5(a)) and enhanced photo emission in optical absorption.

The influence of phonon interaction and its different nature for the two samples can be observed in electric field dependent conductivity and therefore field dependent conductivity is plotted (figure 7). It is observed that for $x = 0$, there is increase in conductivity for $E > 1.6$ kV m^{-1} whereas conductivity for $x = 0.1$ is slightly decreasing showing small trap enhancement in turn leading to slight reduction in mobility. But as the

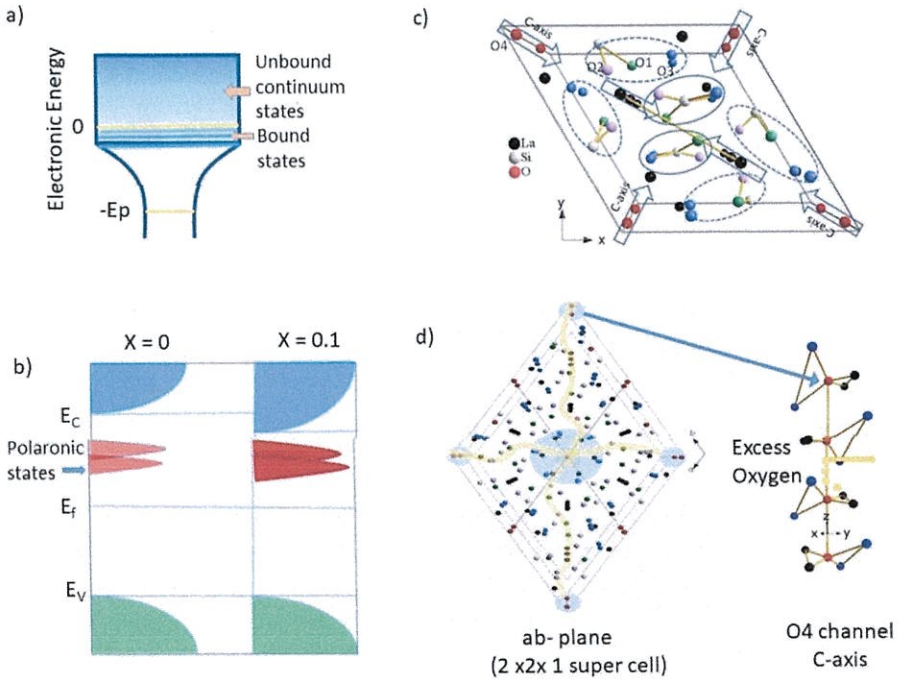

Figure 8. (a) Classical model for bound and unbound continuum states of large polaron self-trapped carrier. (b) Illustration of difference in electronic band structure for $x = 0$ and $x = 0.1$ in $(La^{3+}_{1-x}Ca^{2+}_{x})_{9.67}(SiO_4)^{4-}_{6}O^{2-}_{2+\delta}$ system and polaronic states (c) unit cell structure in the x–y plane in this c-axis is into plane at corner occupied by O4 and surrounded by La1(6 h) site as mentioned earlier (d) $2 \times 2 \times 1$ supercell the long channel formation in *ab*-plane and increase in conductivity in apatite structure (O4–La1(6 h) hexagon can be visualise in central gray oval).

conductivity for $x = 0.1$ is still 100 times higher than $x = 0$ (see figure 7 inset), this suggests higher mobility confirming the formation of large polarons.

3. Discussion

$(La^{3+}_{1-x}Ca^{2+}_{x})_{9.67}(SiO_4)^{4-}_{6}O^{2-}_{2+\delta}$ system shows push–pull and interstitial conduction mechanism governed with the formation of long pathways in O4 column. So far, in ionic solids, the evidences of structural disorder with ionic conductivity are least explored. In addition, like other ionic solids LSO is seen to have wide band gap of ~4.2 eV and therefore ultra wide band gap materials. In the ionic solids, the transport of large polarons at localised sites is coherent in adiabatic limits, which is similar to the motion of fermions in the delocalised states (but slower), therefore large polarons transport can be described in Drude-like formalism (conductivity as a function of low frequency, i.e. order of kHz). Our low frequency dependent conductivity study suggests that the conduction is occurring via overlapping large polaron tunnelling mechanism which can be explained through the classical model for bound and unbound continuum states of large polaron self-trapped carrier as explained earlier in section C and here illustrated in figure 8(a). From the optical absorption and photoemission studies, we can estimate the electronic band structure. Figure 8(b) shows the difference between valence band and conduction band edge with fermi level and polaronic states and it can be seen that for $x = 0.1$, the conduction band is shifted towards the polaronic states rather than for $x = 0.0$. Moreover, the density of polaronic states is higher for $x = 0.1$ than $x = 0.0$. Though Ca substitution at La site does not alter the structure significantly (negligible lattice alteration for $x = 0.1$, which can be attributed to comparable ionic radii of Ca^{2+} as compared to La^{3+}(see supplementary figure S2)) but creates hole polarons. These hole polarons densify the polaronic states significantly. Figure 8(c) shows unit cell structure in the x–y plane in this c-axis is into plane at corner occupied by O4 and surrounded by La1(6 h) site as mentioned earlier and can be visualise in central grey oval in $2 \times 2 \times 1$ supercell (figure 8(d)). Interestingly La2(4f) is almost collinear (~179.9°) along the c-axis. Our study suggests the probability of Ca-substitution on the La2 site is more. Thus without proper grain alignment in the c-axis [42], mixed-channel conduction is achieved by suitable alteration of La2 site and hopping of oxygen is governed between the localized states generated due to La vacancies and oxygen content (long range diffusion in *ab*-plane by La vacancies and excess O ions). With the creation of La vacancies and hole polarons, hopping energy reduces. Further, scattering coefficient (SC) due to optical phonon scattering is reduced to ~1/2 while acoustic phonon scattering is reduced to nearly ~1/4 for $x = 0.1$. This explains the larger tunneling distance and phonon amplitude enhancement for $x = 0.1$ in spite of having same activation and large polarons binding energy. Figure 8(d) illustrates the long channel formation in *ab*-plane and the vacancy diffusion of oxide ion in *a*–*b* plane apart from possible *c*-channel motion.

4. Concluding remarks

The lanthanum excess lanthanum silicate oxyapatite has shown higher oxide ion conductivity with lower activation energy and the activation energy increases with La vacancies (La at 4f site). We have obtained La deficient and O rich samples with Ca substitution (Ca has entered La vacancies and we believe that it has occupied La 4f site). Further, XPS and TGA confirm the formation of La deficient samples. The La(6h)–O4 bond length maximum at $x = 0.1$ suggests the formation of big La (6h) triangles that surround the O4 channel. The Si and O content is observed to increase and O vacancy is observed to decrease with the increase in x. Further, Na-KLL Auger peak of O diminishes with x. Simultaneously, intensity of satellite peak in Ca is increasing with x due to metal ligand interaction, i.e. interaction of s-orbital of Ca and p-orbital of O (s–p interaction). The conductivity, due to connected grain growth increased for $x = 0.1$ which is higher than earlier report with Ca substitution can be attributed to the different local disorder by La and O occupancy. The conduction is occurring via overlapping large polaron tunneling and the potential barrier is generated by the excess oxide ions that can show long range diffusion in the *ab*-plane through interstitials and La2 vacancy creation. This hopping of oxygen is governed between the localized states generated between La vacancies and oxygen content as the interatomic spacing is higher than La1–O3 bond lengths for the samples. Further, the polaron radii reduce with Ca substitution and larger the polaron radius, higher will be the frequency exponent. This is showing the overlap of potential wells of the neighbouring sites (occupied and unoccupied sites) because of long range Coulomb interaction. Thus, with the creation of La-vacancies, hopping energy is reduced for $x = 0.1$. We found that for $x = 0.0$, scattering coefficient (SC) due to optical phonon scattering is reduced to $\sim 1/2$ while acoustic phonon scattering is reduced to nearly $\sim 1/4$ for $x = 0.1$. This study suggests that in apatite structure, ion conduction can be enhanced due to large polaron formation via phonon amplitude enhancement.

4.1. Materials and methods

4.1.1. Sample preparation. Apatite based material lanthanum silicates (LSO) and calcium (Ca) doped LSO were prepared using solid state route method. The starting materials were La_2O_3 (Sigma-Aldrich 99.9%), SiO_2 (Sigma-Aldrich 99.5 %) and $CaCO_3$ (99%) and weighed in stoichiometric proportions. The samples were thoroughly ground using mortar and pestle for 30–40 min. The obtained product was mixed with propanol and ball milled using zirconia ball for 6 h. After ball milling the dried powder was calcined at 1000 °C for 8 h and phase determination of the calcined powder was done. Further, calcined powder was then ground and mixed with Polyvinyl alcohol (PVA) as a binder and pressed at 7 MPa to turn for pelletization and pellets were then sintered at 1375 °C for 14 h at the heating rate of 5° min^{-1}.

4.1.2. Characterization techniques. The phase identification of calcined powder and sintered pellets was done through Rigaku Miniflex powder diffractometer with Cu-Kα radiation (λ = 1.540 598 Å) and Ni filter in the range $2\theta \sim 20$–80° with a step size of 0.02°. The XRD data was refined with $P6_{3/m}$ symmetry using FullProf Suite software package in structural Rietveld mode. After applying zero correction of the instrument, pseudo-Voigt peak profile was used for refinement. The structure is studied using Diamond 3.0 software and bond distances along with lattice parameters are obtained. Further, bond valence sum calculation is done using Full Prof software to find the percolation energy. The thermogravimetric analysis of the calcined powders was carried out simultaneous TG-DSC (Mettler Toledo, Germany) thermal analyzer in the temperature range 30 °–1000 °C at a constant heating rate of 10 °C min^{-1} in the nitrogen atmospheres. The density of prepared sintered pellets was measured using density kit (Sartorius, BSA2245CW). The elemental compositions (EDAX) of the sintered pellets were characterized using scanning electron microscopy (EVO—Scanning Electron Microscope MA15/18). The average grain size was calculated using the linear intercept method. The electrical measurements was done using LCR meter (Wayne Kerr 6500P) in the temperature range 100 °C to 700 °C over the frequency range of between 20 Hz and 1 MHz. The elemental composition was further verified using x-ray photoelectron spectroscopy (Kratos Amicus model) high performance analytical instrument utilizing Mg target under 10^{-6} Pa pressure. The UV–VIS absorption study was carried out using JASCO V-770 ultraviolet–visible (UV) spectrometer. The current–voltage (*I–V*) curve measurement is performed using Keithley 2450 source meter.

Data availability statement

The data that support the findings of this study are available upon reasonable request from the authors.

Acknowledgment

P A J is thankful to CSIR-SRA (13(9142-A)/2020-pool).

Conflict of interest

The authors have no conflicts to disclose.

ORCID iDs

Priyanka A Jha https://orcid.org/0000-0001-7669-5521
Pardeep K Jha https://orcid.org/0000-0001-7048-6147
Prabhakar Singh https://orcid.org/0000-0001-5104-0131

References

[1] Kilner J A, Druce J and Ishihara T 2016 Electrolyte *High-Temperature Solid Oxide Fuel Cells for the 21st Century Fundamentals, Design and Applications* 2nd edn

K Kendall and M Kendall (Amsterdam: Elsevier) (https://doi.org/10.1016/B978-0-12-410453-2.00004-X)
[2] Shi H, Su C, Ran R, Cao J and Shao Z 2020 *Prog. Nat. Sci.: Mater. Int.* **30** 764–74
[3] Nakayama S, Kageyama T, Aono H and Sadaoka Y J 1995 *Mater. Chem.* **5** 1801–5
[4] Verma O N, Jha P K and Singh P 2017 A structural–electrical property correlation in A-site double substituted lanthanum aluminate *J. Appl. Phys.* **122** 22
[5] Verma O N, Jha P A, Singh P, Jha P K and Singh P 2020 Influence of iso-valent 'Sm' double substitution on the ionic conductivity of $La_{0.9}Sr_{0.1}Al_{0.9}Mg_{0.1}O_{3-\delta}$ ceramic system *Mater. Chem. Phys.* **241** 122345
[6] Singh P, Jha P K, Sinha A S K, Jha P A and Singh P 2020 *Solid State Ion.* **345** 115158
[7] Yoshioka H 2007 *J. Am. Ceram. Soc.* **90** 3099–105
[8] Yoshioka H, Nojiri Y and Tanase S 2008 *Solid State Ion.* **179** 2165–9
[9] Laura L-R, Enrique R L, María M-L, Sebastián B and Miguel A G A 2004 *J. Mater. Chem.* **14** 1142–9
[10] Vincent A, Beaudet-Savignat S and Gervais Bruneton F 2007 *J. Eur. Ceram. Soc.* **27** 1187–92
[11] Kobayashi K and Sakka Y 2014 *J. Ceram. Soc. Japan* **122** 921–39
[12] Nojiri Y, Tanase S, Iwasa M, Yoshioka H, Matsumura Y and Sakai T 2010 *J. Power Sources* **195** 4059–64
[13] Lambert S, Vincent A, Bruneton E, Beaudet-Savignat S, Guillet F, Minot B and Bouree F 2006 *J. Solid State Chem.* **179** 2602–8
[14] Beaudet-Savignat S, Vincent A, Lambert S and Gervai F 2007 *J. Mater. Chem.* **17** 2078–87
[15] Fukuda K, Asaka T, Okino M, Berghout A, Béchade E, Masson O, Julien I and Thomas P 2012 *Solid State Ion.* **217** 40–45
[16] Fukuda K, Watanabe R, Oyabu M, Hasegawa R, Asaka T and Yoshida H 2016 *Cryst. Growth Des.* **16** 4519–25
[17] Ogura Y, Yokoi T, Fujii K, Yashima M and Matsunaga K 2022 *J. Phys. Chem.* C **126** 5805–12
[18] Matsunaga K and Toyoura K 2012 *J. Mater. Chem.* **22** 7265–73
[19] Kobayashi K, Hirai K, Uchikoshi T, Sakka Y, Akashi T and Suzuki T S 2021 *Open Ceram.* **6** 100100
[20] Zhao Y, Dai L, Zhangxing H, Wang L and Caoa J 2020 *Ceram. Int.* **46** 5420–9
[21] Cao X G and San Ping J 2014 *J. Mater. Chem.* A **2** 20739–47
[22] Ide S, Takahashi H, Yashima I, Suematsu K, Watanabe K and Shimanoe K 2020 *J. Phys. Chem.* C **124** 2879–85
[23] Kouta I, Toyoura K, Nakamura A and Matsunaga K 2015 *J. Phys.: Condens. Matter* **27** 365601
[24] Nakayama S, Ikesue A, Higuchi Y, Sugawara M and Sakamoto M 2013 *J. Eur. Ceram. Soc.* **33** 207
[25] Emery J, Bohnke O, Fourquet J L, Buzaré J Y, Florian P and Massiot D 1999 *J. Phys.: Condens. Matter* **11** 10401–17
[26] Anisimov V I, Zaanen J and Andersen O K 1991 *Phys. Rev.* B **44** 943–54
[27] Kick M, Scheurer C and Oberhofer H 2021 *ACS Appl. Energy Mater.* **4** 8583–91
[28] Wakamura K 1997 *Phys. Rev.* B **56** 594
[29] Bindi L, Evain M, Pradel A, Albert S, Ribes M and Menchetti S 2006 *Phys. Chem. Miner.* **33** 677–90
[30] Jonscher A K 1983 *Dielectric Relaxation in Solids* (London: Chelsea Dielectrics Press)
[31] Bidault O, Maglione M, Actis M, Kchikech M and Salce B 1995 *Phys. Rev.* B **52** 4191–7
[32] Jha P K, Jha P A, Singh V, Kumar P, Asokan K and Dwivedi R K 2015 *J. Appl. Phys.* **117** 024102
[33] Moreira Toja R J, Rendtorff N M, Agliettia E F, Uchikoshi T, Sakka Y and Suárez G 2018 *Ceram. Int.* **44** 14348–54
[34] Singh P, Jha P K, Jha P A and Singh P 2020 *Int. J. Hydrog. Energy* **45** 23378
[35] Elliott S R 1987 *Adv. Phys.* **36** 135–217
[36] Long A R 1982 *Adv. Phys.* **31** 553
[37] Long A R, Balkan N, Hogg W R and Ferrier R P 1982 *Phil. Mag.* B **45** 497
[38] Emin D and Holstein T 1976 *Phys. Rev. Lett.* **36** 323
[39] Emin D 1993 *Phys. Rev.* B **48** 13691
[40] Imada M, Fujimori A and Tokura Y 1998 Metal–insulator transitions *Rev. Mod. Phys.* **70** 1039
[41] Saurabh Y K, Jha P A, Dubey P K, Jha P K and Prabhakar S 2022 *J. Appl. Phys.* **131** 023106
[42] Bharti P C, Jha P K, Jha P A and Singh P 2021 *J. Phys. Condens. Matter* **33** 155703

R. J. COLLEGE of Arts, Science & Commerc

(Hindi Vidya Prachar Samiti's RAMNIRANJAN JHUNJHUNWALA COLLEG

Opp Ghatkopar Railway Station, Ghatkopar (W), Mumbai 400086, Maharashtra, INDIA

Tel No: +91 22 2515 2731/1763 Fax No: +91 22 25150957 Website: www.rjcollege.edu.in Email: rjcollege@rjcollege.ed

29

14/9/2016

Ref No 2023

To

Shri Yadav AshishKumar Subhash

House No.12, Amaranth Tiwari Chawl

Pratap Nagar, Caves Road

Jogeshwari (E), Mumbai 400 060

Subject: Letter of Appointment as Assistant Professor in Ramniranjan Jhunjhunwala College, Ghatkopar (W), in the subject of Physics

Dear Sir,

The Governing Body of Ramniranjan Jhunjhunwala College of Arts, Science and Commerce is pleased to inform you that you have been appointed on probation as a Assistant Professor in the subject of Physics of the aforesaid college with effect from 16th September, 2016 in the pay scale of Rs. 15600-39100 AGP Rs. 6000 with other allowances as admissible.

Your appointment is subject to approval from University of Mumbai and the Joint Director's Office, Mumbai Region.

Your appointment is on probation for one year which is extendable to two years depending on your performance appraisal. During the period of probation your services can be discontinued by giving one month notice on either side.

Your services will be governed by the provisions of the Mumbai University Acts-1974, 1994 and Maharashtra University Act 1994 and the statutes and Regulations of the University of Mumbai.

You are required to give your acceptance letter in writing.

Yours Sincerely

Usha

Dr Usha Mukundan

Principal

PRINCIPAL
RAMNIRANJAN JHUNJHUNWALA COLLEGE
GHATKOPAR, MUMBAI-400 086.

Received
Yadav